Available online at www.sciencedirect.com
ScienceDirect
Journal of Hydrodynamics
2009,21(5):600-607
DOI: 10.1016/S1001-6058(08)60190-0
www.sciencedirect.com/science/journal/10016058

DIRECT NUMERICAL SIMULATION OF TURBULENT FLOW IN A STRAIGHT SQUARE DUCT AT REYNOLDS NUMBER 600*

ZHU Zuo-jin
Multiphase Reactive Flow Division, Department of Thermal Science and Energy Engineering, University of Science and Technology of China, Hefei 230026, China, E-mail: zuojin@ustc.edu.cn
YANG Hong-xing, CHEN Ting-yao
Department of Building Services Engineering, The Hong Kong Polytechnic University, Hong Kong, China

(Received October 26, 2007, Revised March 8, 2008)

Abstract: This article presents the direct numerical simulation results of the turbulent flow in a straight square duct at a Reynolds number of 600, based on the duct width and the mean wall-shear velocity. The turbulence statistics along the wall bisector is examined with the turbulent flow field properties given by streamwise velocity and vorticity fields in the duct cross section. It was found that the solutions of the turbulent duct flow obtained in a spatial resolution with 1.2×10^6 grid points are satisfactory as compared to the existing numerical and experimental results. The results indicate that it is reasonable to neglect the sub-grid scale models in this spatial resolution level for the duct flow at the particular friction Reynolds number.

Key words: straight square duct, turbulent flow, direct numerical simulation

1. Introduction

Turbulent flow in a straight square duct has a remarkable change in flow structure that results in the so-called Prandtl's second kind secondary flows with the velocities generally much higher than those induced by turbulence[1]. Gessner in his early experiments[2] examined the mechanism of initiate secondary flow in developing turbulent flow along a corner. He applied both energy and vorticity balance to the mean motion along a corner bisector. His results indicated that a transverse flow is initiated and directs towards the corner as a direct result of turbulent shear stress gradients normal to the bisector. Moreover, the anisotropy of the turbulent normal stresses did not play a major role in the generation of secondary flow. The recent experiment conveyed the observation of the effects of the secondary flow in a square duct on mass transfer near the corners. The effects were initially small, but grew to a significant degree further downstream[3].

The numerical studies in this area started relatively later than the experimental studies that were initially carried out in 1960s and 1970s. Nakayama et al. [4] presented an algebraic stress model combined with the $k-\varepsilon$ model for simulating the secondary flow of the second kind and conducted numerical simulation of fully developed turbulent flows in square, rectangular and trapezoidal ducts. They made an intensive comparison between their numerical results and the available experimental data, and particularly emphasized the local structure of turbulence to reveal the full features of this stress model. The numerical work of Demuren and Rodi[5] have shown that the main features of the mean-flow

* Project supported by the National Natural Science Foundation of China (Grant No. 10572135), the Research Grants Council of the Hong Kong Special Administrative Region, China (Grant No. PolyU5130/04E).
Biography: ZHU Zuo-jin (1962-), Male, Ph. D., Associocte Professor

and the turbulence quantities can be simulated realistically, but the secondary velocity is dependent on turbulence models.

Recently, with the development of computer technology, the Direct Numerical Simulation (DNS) has become a tool in turbulence study for flow at a low Reynolds number. Liu et al.[6] have investigated the turbulent open channel flows subjected to the control of a spanwise travelling wave to reveal the response of the near-wall and surface-influenced turbulence to the spanwise travelling wave control. Some typical quantities, including the mean velocity, velocity fluctuations and the structures of turbulence fluctuations, are exhibited and analyzed.

Gavrilakis[7] has presented the DNS results for the turbulent flow in a straight duct at a Reynolds number of 300, based on the mean-wall shear velocity and the duct width. His turbulence statistics along the wall bisectors agreed well with plane channel flow data despite the influence of the sidewalls in the duct flow. Joung et al.[8] performed the DNS of turbulent flow in a square duct at the same $Re = 300$ recently. Their results indicated that the two counter-rotating secondary flows around the duct corner play a key role in momentum transfer between the corner and the centre of the duct. Huser and Biringen[9] carried out the DNS of a fully developed turbulent duct flow at a relatively high Reynolds number of 600 (based on the mean wall-shear velocity and the duct width). They found that the mean secondary flow pattern, the distorted isotachs and the anisotropic Reynolds stress distribution could be explained by the preferred location of an ejection structure near the corner and the interaction between bursts from the two intersecting walls. The corner effects were also manifested in the behaviour of the pressure-strain and velocity-pressure gradient correlations. A more recent coarse grid DNS of air flow in a straight square duct at a friction Reynolds number 400 and heat transfer was conducted by Liang et al.[10]. It was concluded that the resolution of discretization of the momentum equations is a key feature for the turbulent duct flow simulation.

This article presents the DNS results of the fully developed turbulent duct flow for the same case investigated by Huser and Biringen[9]. However, emphasis is laid on the calculation of turbulence statistics including the main-flow variables, the root mean square and the skewness as well as flatness factors of velocity fluctuations along the wall bisectors. This is because it has been noticed that the higher order turbulence statistics for duct flow has not been highlighted in the previous works[7,9]. It is well known that the DNS is a research tool rather than a brute-force solution to the Navier-Stokes equations for engineering problems[11]. Hence, this numerical work is to verify that for the turbulent square duct flow at the Reynolds number of 600, satisfactory results can be obtained when the spatial resolution of 1.2×10^6 (= $121\times101\times101$) grid points is used and the sub-grid scale models are neglected.

2. Governing equations and numerical methods

2.1 *Governing equations*

The origin of global coordinate was arranged at the center of the computational domain, and the duct-half width h and the mean wall-shear velocity u_τ with a constant factor of a_1 were taken as the length and velocity scales, respectively. Thus, the mean driving pressure gradient of the duct flow can be expressed by $2/a_1^2$. Denote the Reynolds number by $Re_s = ha_1u_\tau/\nu = 0.5a_1Re_\tau$, with ν representing the fluid kinematic viscosity, then the governing equations of the fully turbulent flow in a square duct can be written as

$$\frac{\partial u_i}{\partial x_i} = 0 \tag{1}$$

$$\frac{\partial u_i}{\partial t} + u_j\frac{\partial u_i}{\partial x_j} = -\frac{\partial p}{\partial x_i} + \delta_{1i}\frac{2}{a_1^2} + \frac{1}{Re_s}\frac{\partial^2 u_i}{\partial x_j^2} \tag{2}$$

The finite difference solutions in the computational domain can be sought using periodic boundary conditions in the main flow direction with a period of 12.824 and non-slip boundary condition on the duct walls when the initial field is obtained by disturbing a laminar duct flow. The turbulence statistics is calculated in the time range from 180 to 280 when the duct flow is regarded as statistically steady. The time unit is given by $h/(a_1u_\tau)$.

2.2 *Numerical methods*

The accurate projection algorithm PmIII developed by Brown et al.[12] was used in the present DNS using a non-uniform staggered grid. The intermediate velocity was calculated excluding the pressure gradient terms, and the convective terms were calculated explicitly in terms of the second-order Adams-Bashforth scheme in time. In the calculation of the intermediate velocity, the present DNS did not follow the fractional methods of Gavrilakis[7], Huser and Biringen[9] which merged the streamwise diffusion terms into the convective terms, but employed the block-tridiagonal technique with respect to the streamwise periodic condition. The block-tridiagonal technique was also used in the calculation of the pressure potential.

Specifically, a fourth-order upwind scheme based on the Taylor expansion was used to discretize the nonlinear convective terms in the governing equations. This finite difference approximation scheme was detailed in the wake flow simulation work of Niu and Zhu[13]. The pressure potential field was predicted by the approximate factorization one (AF1) scheme reported by Baker[14], which was also used previously in the simulation of laminar natural convection in a tall cavity[15] and the turbulent Rayleigh-Benard convection[16]. The maximum iterative acceleration factor in AF1 was given in accord to the nearest grid spacing to the wall, i.e. $4/(\delta y)^2_{\min}$, and the minimum acceleration factor was assigned as unity. Each iterative cycle had six steps with different iterative acceleration factors changing from its maximum to minimum. The convergence criterion of the AF1 iteration was $\|\Delta\phi\|/(\|\phi\|+10^{-4})$ whose value should be smaller than 10^{-6}, where ϕ represents the pressure potentials relevant to p in the accurate projection method.

Table 1 Calculated mean velocity u^+ in near-wall region

y^+	u^+	y^+	u^+
0.168	0.17057	6.954	5.98358
0.366	0.34907	8.349	7.02624
0.6	0.55878	9.993	8.14786
0.876	0.80509	11.925	9.31559
1.2	1.09425	14.196	10.4876
1.578	1.43354	16.872	11.6212
2.028	1.83125	20.016	12.6820
2.553	2.29678	23.718	13.6488
3.174	2.84039	28.074	14.5111
3.903	3.47268	33.195	15.2675
4.758	4.20353	39.222	15.9237
5.766	5.04004	46.314	16.4920

3. Results and discussion

The DNS of the turbulent flow in a square duct was carried out in a personal computer with a memory of 1 Gb. The time step Δt in the unit of $h/(a_1 u_\tau)$ was set as 0.008. The data used for turbulence statistics calculation was sampled with a definitive time interval of $10\Delta t$ and in the time range from 180 to 280. The CPU time for the data sampling process is 21.5 h. The parameter a_1 was assigned as 13. The nearest grid spacing to the wall was 5.6×10^{-4}. The spatial grids with a number 121×101×101 were staggered for velocity and pressure, and were non-uniformly arranged in the computational domain 12.824×2×2. The grid arrangement in the normal to the wall direction in the near wall region is listed in Table 1. The period in the streamwise direction was set as 12.824. The mean flow properties were used on an average over x and t, in which the range used for the time average was given by $t\in[180,280]$. A prime represents a deviation from this average. The four aspects of calculation results will be discussed in this section, which include the mean flow properties, the turbulence statistics, the power spectra of velocities, and the turbulent flow fields. The experimental data of Niederschulte, Nishino and Kasagi were taken indirectly from the work of Gavrilakis[7] for comparison.

3.1 *Mean flow properties*

The mean flow varaibles based on the present DNS and those reported by Huser and Biringen (1993, hereinafter denoted as HB)[9] are summarized in Table 2, where U_b, U_c are the bulk mean velocity and the mean velocity in the centreline of the square duct, respectively. It can be seen that the values of the mean flow variables agree quite well with the DNS results of HB for the case of duct flow at the same friction Reynolds number of 600.The mean streamwise velocity along the wall bisector in the wall coordinate is shown inFig.1, where the mean velocity profiles obtained at the different Reynolds numbers are illustrated together. It is seen that the profile labelled by solid line collapses with the circles and filled circles, indicating that the present DNS has given rise to favourable mean sreamwise velocity profile along the wall bisector. It is noted that the mean streamwise velocity obtained by Gavrilakis[7] is normalized by the unit of local shear velocity rather than the mean shear velocity. When the flow becomes fully turbulent, the Reynolds number determines the range of logarithmic region of the mean streamwise velocity profile. The the range is increased with increasing Reynolds number.

The values of the calculated mean velocity in the near wall region are given in Table 1. The grid arrangement in this region is characterized by a fixed amplifying factor (20/17) of grid spacing, and the linear law in the region very close to the wall ($y^+ < 5$) is approximately satisfied.

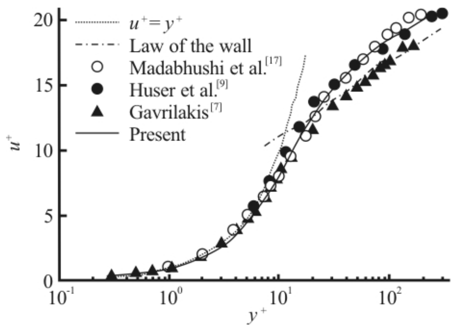

Fig.1 Mean streamwise velocity along the wall bisector in the wall coordinate. Note that the law of the wall is given by $u^+ = 2.5\ln y^+ + 5.5$, where $u^+ = u/u_\tau$, $y^+ = y/(\nu/u_\tau)$, the velocity from the DNS of Gavrilakis[7] is normalized by the local wall-shear velocity. The friction Reynolds number for the LES of Madabhushi and Vanka[17] is 360

Table 2 Comparison of mean flow properties

Variable	Huser et al.[9]	Present
$Re_\tau = 2u_\tau h/\nu$	600	600
$Re_b = U_b 2h/\nu$	10320	9960
U_b/u_τ	17.21	16.61
$\overline{f} = 8\overline{\tau}_w/(\rho U_b^2)$	0.027	0.029

3.2 *Turbulence statistics*

The turbulence statistics for fully developed flow in a straight square duct includes the root-mean square (rms) values of velocity fluctuations, the correlation coefficient of u' and v', and the skewness and flatness factors of velocities. Showing the statistics of turbulence of the duct flow is useful for the detailed understanding of the velocity fluctuation properties. In particular, calculating the skewness and flatness factors is helpful to know the flow heterogeneity, while giving the rms values is helpful to know the velocity fluctuating amplitude in the three spatial directions, and the turbulent diffusivity that further related to the velocity correlation coefficient. The corresponding results can be observed in Figs.2, 3, 4 and 5.

The turbulence intensities (or rms values of velocities) labelled by squares in Figs.2(a)-2(c) are the experimental results of Kreplin and Eckelmann (1979, hereinafter denoted as KE)[18], which are relevant to the turbulent channel flow at $Re_\tau = 192$ (based on the channel half width and the mean wall-shear velocity). While those labelled by triangles are the measured results given by Balint et al.[19] for a turbulent boundary layer. In addition, for the convenience of comparison, the DNS results for channel flow at a friction of 180 of Kim, et al. (1987, hereinafter denoted as KMM)[20] are labelled by filled circles, with the results of HB and Gavrilakis[7] labelled by circles and plus-symbols respectively.

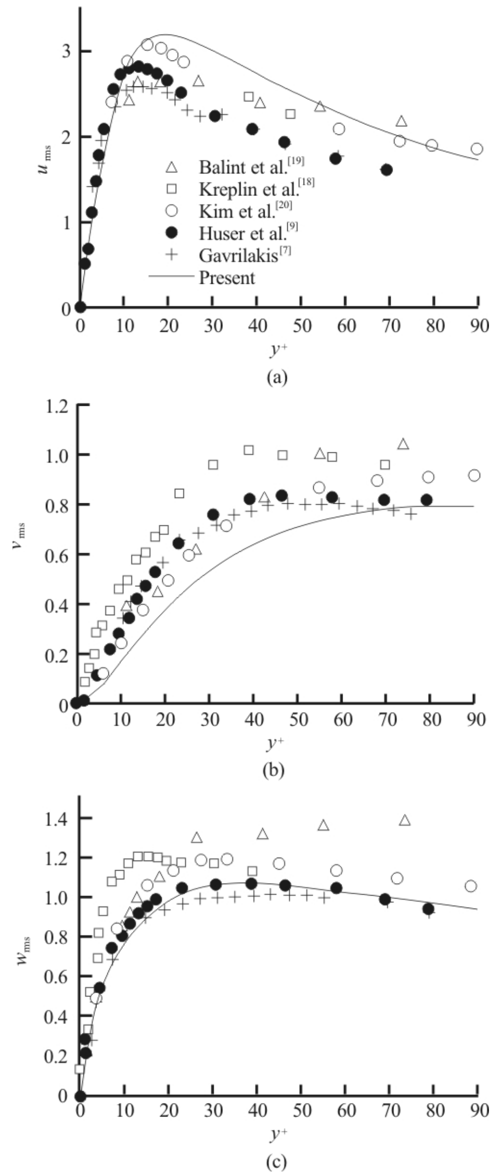

Fig.2 Root mean square values of velocities along the wall bisector in the wall coordinate

It should be noted that the velocity fluctuations to some extent depend on the accuracy of the numerical scheme used in discretization, since the finite difference schemes suffer from the effects of numerical viscosity and dispersion, and there are numerical error patterns even for transient one-dimensional linear wave equations[21]. It is also noted that for the thermal-induced turbulence in a differentially heated air-filled cavity, even for using a spectral method, it seems that the second-order treatment of the convective terms is responsible for the failure of correct prediction of the Reynolds shear stress along the bisector of the heating and cooling walls[22]. This is why the fourth-order upwind scheme is adopted in the present DNS. Examination of the DNS results of HB shows that the turbulence intensities are also dependent on the computation method, and it indicates that there is a fairly good agreement between them. The numerical results have qualitative consistency with the experimental results of KE and Balint et al..

On the other hand, as is shown in Fig.3, the curve of the correlation coefficient of u' and v' along the wall bisector in the global coordinate is in a good agreement with both the calculated and measured results. The data measured by Sabot and Comte-Bellot[23] is relevant to a circular pipe flow at much higher Reynolds number (from 6.8×10^4 to 1.35×10^4, based on the centreline velocity and the pipe diameter). The results show that the correlation coefficient is almost independent of both the Reynolds number and the computation method.

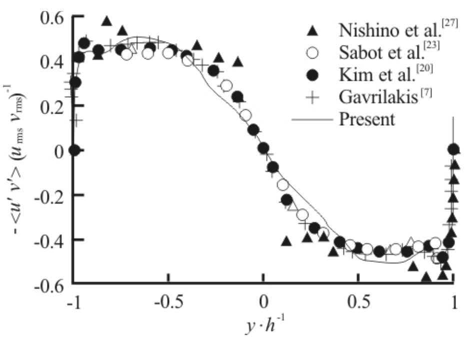

Fig.3 Correlation coefficient of u' , v'

Since the skewness factor of the velocity fluctuation in the spanwise direction along the wall bisector is close to zero, in Figs.4(a)-4(b), only $S(u')$ and $S(v')$ are plotted as functions of the global coordinate along the wall bisector. It can be seen, from Fig.4(a), that the skewness factor $S(u')$ is in good consistency with the results of channel flows (KE and KMM), with noticeable discrepancy appearing at the core region of the duct flow ($|y/h|<0.5$) as compared with the DNS results of KMM. With respect to the DNS results of Gavrilakis, it indicates that the effects of the Reynolds number and solution method on the skewness factor $S(u')$ are not significant. However, these effects on the distribution of the skewness factor $S(v')$ along the wall bisector are significant (see Fig.4(b)). It is noted that the skewness factor $S(v')$ labelled by the solid line in the present calculation shows a tendency of collapsing with the measured data of KE particularly in the near-wall region. While in the core region, it shows a good agreement with the measured data of Niederschulte[24]. As is shown in Fig.4(b), it is noted that the calculated $S(v')$ is in a fairly good agreement with the DNS results of KMM and Gavrilakis.

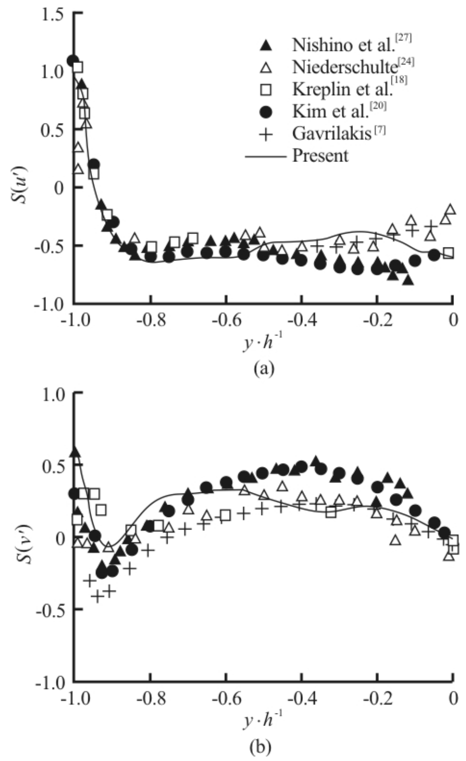

Fig.4 Skewness factors of velocity along the wall bisector in global coordinate

A comparison between the distribution of flatness factors along the wall bisector and the corresponding results of KMM for a turbulent channel flow is presented in Fig.5. Again, a noticeable discrepancy occurs in the core region of the flatness factors $F(u')$, $F(w')$, but for the flatness factor $F(v')$, the discrepancy appears in the vicinity of the wall.

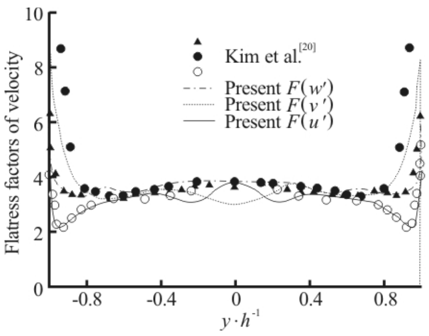

Fig.5 Flatness factors of velocity along the wall bisector in global coordinate

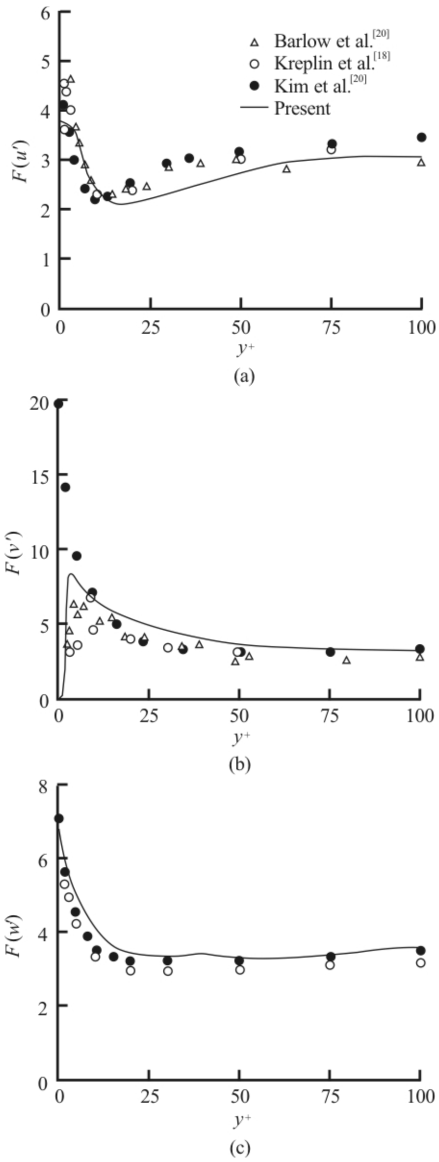

Fig.6 Flatness factors along the wall bisector in wall coordinate. The data labeled by Barllow et al. are abstracted from Ref.[20]

Another detailed comparison between the distribution of the flatness factors in a wall coordinate and the existing data (in the works of KE, KMM, and Barllow et al.) is shown in Figs.6(a)-6(c). It suggests that both the sidewall and the Reynolds number have no significant effects on the flatness factor along the wall bisector. The flatness factor $F(u')$ at the wall is around 3.5, a value reported by KE.

3.3 *Flow fields*

The turbulent flow fields are shown in Figs.7(a)-7(b) and 8(a)-8(b) in the cross section at $x = 0$ at two different moments ($t = 260$, 280). The turbulence-induced instantaneous secondary flows given in Fig.7 contain asymmetrical vortical structures with coherent flow patterns near the walls. These patterns are quite similar to the flow fields given by velocity vectors obtained at a lower Reynolds number[8]. The asymmetry of flow structures may come from the break-up of the traveling waves occurred in the flow transition period[25], whose mechanism is involved with the non-linear dynamics.

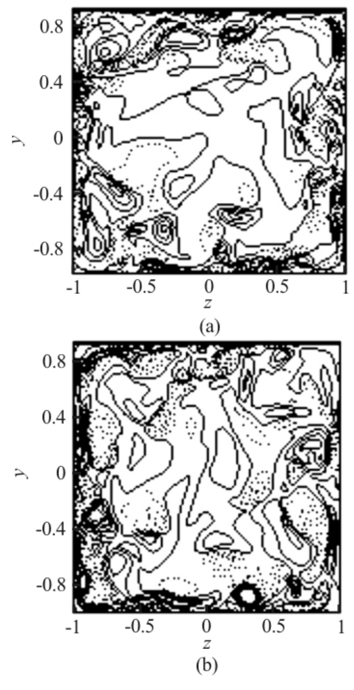

Fig.7 Instantaneous contours of streamwise vorticity in the cross-section of $x = 0$. Note that the vorticity contours are labelled by values from -4 to 4, with a vorticity increment of 0.8

These secondary motions correspond to the streamwise velocity fields shown in Figs.8(a)-8(b). The streamwise velocity fields contain the pattern in the core region consisting of transient array of plateaux separated by sharp cliffs similar to observed in scalar turbulence[26], and the wrinkled pattern near the wall, as shown in Figs.8(a)-8(b), suggesting that the duct flow has certainly become fully turbulent. Note that the velocity is labelled by values from 0.1 to 1.6 u_s, here $u_s = 13u_\tau$.

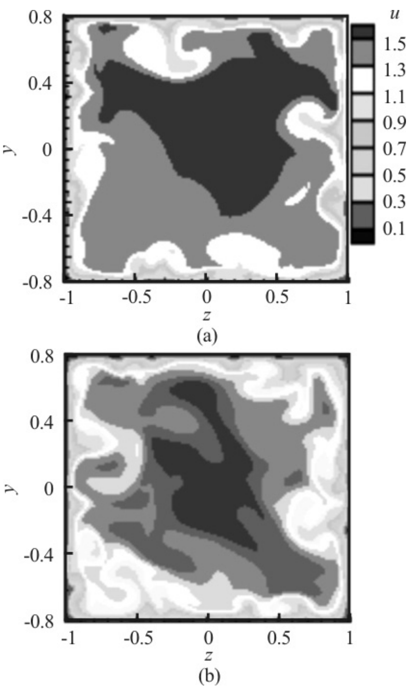

Fig.8 Contours of streamwise velocity in the cross-section of $x = 0$

4. Conclusion

DNS of fully developed turbulent flow in a straight square duct at a friction Reynolds number of 600 has been carried out using finite difference approximation. The DNS work on the staggered grid of number 1.2×10^6 has been focused on the calculation of the turbulence statistics including the rms values, the skewness and flatness factors of velocity fluctuations along the wall bisector. The comparison of the DNS results with the existing numerical and experimental data shows satisfactory consistence, indicating that for the duct flow at the particular friction Reynolds number of 600, when the spatial resolution is achieved at the level of about 10^6, and neglecting the sub-grid scale model is probably reasonable. The instantaneous secondary flow fields show asymmetrical vertical structures which may come from the break-up of travelling waves that appear in the flow transition period, with the mechanism of wave break-up associated with nonlinear dynamics.

Acknowledgement

We thank Professor Liu Ying-zhong at Shanghai Jiao Tong University for useful communications.

References

[1] BRADSHAW P. Turbulent secondary flows[J]. **Ann. Rev. Fluid Mech.,** 1987, 19(1): 53-74.

[2] GESSNER F. B. The origin of secondary flow in turbulent flow along a corner[J]. **J. Fluid Mech.,** 1973, 58: 1-25.

[3] GOLDSTEIN R. J., YABBARI M. Y. and BREKKE J. P. The near-corner mass transfer associated with turbulent flow in a square duct[J]. **Heat Mass Transfer,** 1992, 27(4): 265-272.

[4] NAKAYAMA A., CHOW W. L. and SHARMA D. Calculation of fully developed turbulent flows in ducts of arbitrary cross-section[J]. **J. Fluid Mech.,** 1983, 128: 199-217.

[5] DEMUREN A. O., RODI W. Calculation of turbulence-driven secondary motion in non-circular ducts[J]. **J. Fluid Mech.,** 1984, 140: 189-222.

[6] LIU Nan-sheng, WANG Lei and LU Xi-yan. Turbulent open channel flow subjected to the control of a spanwise travelling wave[J]. **Journal of Hydrodynamics,** 2009, 21(1): 65-70.

[7] GAVRILAKIS S. Numerical simulation of low-Reynolds-number turbulent flow throuth a straight square duct[J]. **J. Fluid Mech.,** 1992, 244: 101-129.

[8] JOUNG Y., CHOI S. U. and CHOI J. I. Direct numerical simulation of turbulent flow in a square duct: Analysis of secondary flows[J]. **ASCE, J. Engng. Mech.,** 2007, 133(2): 213-221.

[9] HUSER A., BIRINGEN S. Direct numerical simulation of turbulent flow in a square duct[J]. **J. Fluid Mech.,** 1993, 257: 65-95.

[10] MA Liang-dong, LI Zeng-yao and TAO Wen-quan. The application of high resolution finite difference scheme in direct numerical simulation of turbulent flow[J]. **J. Engineering Thermophysics,** 2007, 28(5): 859-861(in Chinese).

[11] MOIN P., MAHESH K. Direct numerical simulation: A tool in turbulence research[J]. **Annu. Rev. Fluid Mech.,** 1998, 30(1): 539-578.

[12] BROWN D. L., CORTEZ R. and MINION M. L. Accurate projection methods for the incompressible Navier-Stokes equations[J]. **J. Comput. Phys.,** 2001, 168(2): 464-499.

[13] NIU J. L., ZHU Z. J. Numerical study of three-dimensional flows around two identical square cylinders in staggered arrangements[J]. **Phys. Fluids,** 2006, 18(4): 044106.

[14] BAKER T. J. Potential flow calculation by the approximate factorization method[J]. **J. Comput. Phys.,** 1981, 42(1): 1-19.

[15] ZHU Z. J., YANG H. X. Numerical investigation of transient laminar natural convection of air in a tall cavity[J]. **Heat and Mass Transfer,** 2003, 39(7): 579-587.

[16] YANG H. X., ZHU Z. J. Numerical simulation of turbulent Rayleigh-Benard convection[J]. **Int. Comm. Heat Mass Transfer,** 2006, 33(2): 184-190.

[17] MADABHUSHI R. K., VANKA S. P. Large eddy simulation of turbulence-driven secondary flow in a square duct[J]. **Phys. Fluids A,** 1991, 3(11): 2734-2745.

[18] KREPLIN H. P., ECKELMANN H. Behavior of the three fluctuating velocity components in the wall region of a trubulent channel flow[J]. **Phys. Fluids,** 1979, 22(7): 1233-1239.

[19] BALINT J. L., WALLACE J. M. and VUKOSLAVCEVIC P. The velocity and vorticity vector fields of a turbulent boundary layer. Part 2. Statistical properties[J]. **J. Fluid Mech.,** 1991, 228: 53-86.

[20] KIM J., MOIN P., and MOSER R. Turbulence statistics in fully developed channel flow at low Reynolds number[J]. **J. Fluid Mech.,** 1987, 177: 133-166.

[21] ZHU Z. J., WANG X. Q. and SU Z. B. Numerical error patterns for a scheme with hermite interpolation for 1+1 linear wave equations[J]. **Comm. Numerical Method in Engng.,** 2004, 30(5): 353-361.

[22] SALAT J., XIN S. and JOUBERT P. et al. Experimental and numerical investigation of turbulent natural convection in a large air-filled cavity[J]. **Int. J. Heat Fluid Flow,** 2004, 25(55): 824-832.

[23] SABOT J., COMTE-BELLOT G. Intermittency of coherent structures in the core region of fully developed turbulent pipe flow[J]. **J. Fluid Mech.,** 1976, 74: 767-796.

[24] NIEDERSHULTE M. A. Turbulent flow through a rectangular channel[D]. Ph.D. Thesis, Illinois, USA: University of Illinoise at Urbana-Champaign, 1989.

[25] HOF B., Van DOORNE C. W. H. and Westerweel J. et al. Experimental observation of nonlinear travelling waves in turbulent pipe flow[J]. **Science,** 2004, 305(5690):1594-1598.

[26] SHRAIMAN B. I., SIGGIA E. D. Scalar turbulence[J]. **Nature,** 2000, 405(6787): 639-646.

[27] NISHINO K., KASAGI N. Turbulence statistics measurement in a two-dimensional channel flow using a three-dimensional particle tracking velocimeter[C]. **STSF'89, Seventh Symposium On Turbulent Shear Flows.** Palo Alto, California, USA: Stanford University, 1989, 21-23.